International Journal of Engineering Research-Online
A Peer Reviewed International Journal
Articles available online http://www.ijoer.in; editorijoer@gmail.com

Vol.4., Issue.6., 2016
Nov-Dec.

RESEARCH ARTICLE

ISSN: 2321-7758

NUMERICAL SIMULATIONS OF THE CABBELING PHENOMENON IN THERMAL BAR

ALABODITE MEIPRE GEORGE,[1,2] PROMISE MEBINE[2]

[1]Department of Mathematical Sciences, Loughborough University, Leicestershire, United Kingdom
Email: A.M.George@lboro.ac.uk, georgianalgebra@gmail.com

[2]Department of Mathematics/Computer Science, Niger Delta University, Wilberforce Island, Bayelsa State, Nigeria
Email: p.mebine@yahoo.com, pw.mebine@ndu.edu.ng

ABSTRACT

The behaviour of warm water discharges at a temperature higher than maximum density temperature T_m horizontally into a homogeneous body of cold fresh water at a temperature lower than T_m has been investigated by means of the hydrodynamic equations via numerical simulations by COMSOL Multiphysics. Water density was taken to be a quadratic function of temperature, thereby enhancing a Cabbeling process, which was inevitable as the water masses come in contact to form a thermal bar. Rayleigh-Taylor instability in the thermal bar and Kelvin-Helmholtz instability in density current were observed during the simulations. It was also observed that the interaction between the two instabilities causes a deformation in the thermal bar. It was seen that the Rayleigh-Taylor instability was frequently restoring the vertical front of the thermal bar, while the Kelvin-Helmholtz instability destroys the thermal bar whenever it prevails over the Rayleigh-Taylor instability, thereby causing a shift in the thermal bar towards the warm water region. The behaviour of the results as presented in this paper are mostly dependent on the Reynolds and the Froude numbers as they vary.

Keywords —Buoyancy reversal, Cabbeling, Maximum density, Surface current.

I. INTRODUCTION

Hydrodynamic processes are important areas of research and such processes can be found in many practical applications and throughout natural sciences, and they encompass many natural phenomenal behaviours, especially, when water masses with temperatures on either side of the temperature of maximum density (T_m) in fresh water meets. This in turn leads to the formation of different phenomenal behaviours such as, the formation of thermal bar [1], surface or density currents [2, 3] and sometimes a buoyant plume can also experience buoyancy reversal when the discharge is initiated at a greater depth [4, 5]. All these and more are features of hydrodynamic processes.

When these water masses with the temperatures on either side of the temperature of maximum density (T_m) in fresh water come in contact, mixing produces water that is denser than either of the original water masses, a process known as Cabbeling [6, 7]. In this case, it is known

that $T_m = 3.98^0 C$, is the temperature of maximum density for fresh water at atmospheric pressure, and it is approximated as 4°C in most numerical calculations. This behaviour is mostly found in lakes, especially in holomictic lakes, and the point, where the two water masses meet, cabbeling water forms a descending plume that draws in surrounding water, causing a sharp thermal front [1, 8]. This thermal front was first noticed by Forel [9], who called it the barre thermique (thermal bar) as it forms a barrier between water masses with temperature on either side of 4°C. A thermal bar is a hydrodynamic feature that develops within the shores of holomictic lakes during the seasonal transition to stratified conditions, due to the shorter amount of time required for shallow areas of the lake to stratify. During the spring for example, the shallow regions near the shores of a lake, surface water gets warmer because of direct heating from the sun, and this part of the lake will warm faster than the deeper part, due to their smaller volume and additional radiation absorption by the lake bed [10, 11, 12, 13]. If the initial temperature of the lake was below 4°C, then the shallow region will certainly be warmer than 4°C and the deep region cooler; then a thermal bar will be formed between these waters as the mixture is at 4°C and sinks (see Figure 1). Water within the thermal bar sinks until it reaches a depth, where it is no longer denser than the surrounding fluid if the domain has greater depth. This may happen for several reasons, such as entrainment of lower density water into the plume or varying thermal characteristics of the surrounding water. On the other hand, this denser water can descend to the floor and spread out as a density current. More detailed studies on such flows are also presented in [14, 15, 16].

Furthermore, power stations discharge their cooling waste water at a temperature higher than T_m and the receiving water lower than T_m [17 - 20]. The discharged water is, therefore, less dense than the receiving water, if it is released near the surface it will spread out as a gravity current at the surface, but if it is released at a greater depth, it will rise to the surface before spreading outwards as a surface current. Such flows are usually unsteady with some degree of Rayleigh-Taylor instabilities as denser fluid is produced. However, an exception to this may occur if the receiving water is below the temperature of maximum density [2, 21 - 27]. Mixing between the warm water in a surface gravity current and the cold receiving water can then produce water, which is denser than either component, and sinks to the floor, and will then spread along the bed as a dense gravity current. Evidence for this, was found in Lake Michigan by Hoglund and Spigarelli [28], though the authors were only concerned with the biological implications of the spread of warm water along the lake bed, but did not consider the dynamics. Positively buoyant plume and Surface current are different kinds of flow as compared to thermal bar, but the Cabbeling phenomenon that leads to the production of denser fluid or a mixture at the temperature of maximum density before sinking is similar. Density current is also a similar kind of flow to that of the surface current, that is, a consequence of cabbeling or when fluid with maximum density T_m is introduced into a receiving water that is less dense. For the case of the present study, this current is usually observed when denser water descends from the thermal bar to the floor with a leading head displacing the ambient water as it mixes further on the floor.

The aim of this paper is, therefore, to carry out numerical simulations on thermal bar, where water masses of different temperatures are placed in a container, one on the left and the other on the right in the form of a lock exchange method as shown in Figure 2, but with the assumption that the density is a quadratic function of temperature. Cabbeling is only expected at their point of contact, and any water that have mixed up to the temperature T_m or that have become dense is expected to sink. On the floor, denser fluid that have descended will continue to spread as density current. Note that different temperatures can correspond to the same density, in such a situation, neither of the water is expected to flow as a surface or density current at initial times, except for the cabbeling water that descends to the floor as it

becomes denser.

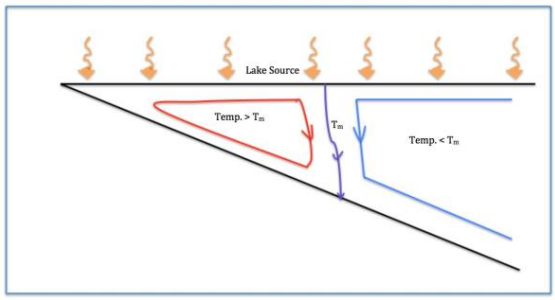

Figure 1: Schematic presentation of spring thermal bar driven by a surface heat input.

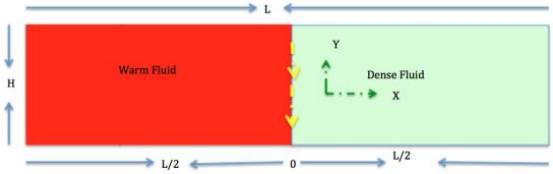

Figure 2: Schematic presentation of Lock-exchange flow in a channel of length L and height H. The yellow dotted line gives the interface between the two fluids sometime after the release.

II MODEL FORMULATION AND GOVERNING EQUATIONS

Behaviour of the thermal bar as denser fluid descends to the floor due to the nonlinear relation between density and temperature T is key and as such, the following relation is appropriate for this investigation:

$$\rho = \rho_m - \beta(T - T_m)^2. \quad (1)$$

This equation gives a very good fit to the experimentally determined density of fresh water at temperatures below 10°C, when it is considered that $T_m = 3.98^0 C$, $\rho_m = 1.000 \times 10^3 kgm^{-3}$ and $\beta = 8.0 \times 10^{-3} kgm^{-3} \left({}^0 C\right)^{-2}$ [30, 31] and all other fluid properties (e.g. viscosity, thermal diffusivity) are assumed constant. It is also assumed that the flow is time-dependent and two dimensional, and that the liquid property is constant except for the water density, which changes with temperature and in turn results to the buoyancy force. In order to facilitate the analyses, the coordinates x, y, velocity components u, v, time t, pressure p and temperature T are rendered dimensionless by

$$U = \frac{u}{v_{in}},\ V = \frac{v}{v_{in}},\ X = \frac{x}{x_{in}},\ Y = \frac{y}{x_{in}},\ \tau = \frac{t}{\left(\frac{x_{in}}{v_{in}}\right)},\ P = \frac{p}{\rho v_{in}^2},\ \phi = \frac{T - T_\infty}{T_m - T_\infty}, \quad (2)$$

where x and u are horizontal, y and v are vertical. The emerging dimensionless parameters: the Reynolds, Re; Prandtl, Pr and Froude, Fr Numbers are defined by

$$\nu = \frac{\mu}{\rho},\ \alpha = \frac{\kappa}{\rho c_p},\ \mathrm{Re} = \frac{v_{in}\, x_{in}}{\nu},\ \mathrm{Pr} = \frac{\nu}{\alpha},\ Fr^2 = \frac{\rho_m v_{in}^2}{g\beta(T_m - T_\infty)^2 x_{in}}, \quad (3)$$

where ν and α are the respective diffusivities of momentum and heat, and μ is viscosity, κ is thermal conductivity and c_p is specific heat capacity at constant pressure.

In terms of these dimensionless variables and parameters, the continuity equation, the horizontal and vertical momentum equations and the thermal energy equation are given as

$$\frac{\partial U}{\partial X} + \frac{\partial V}{\partial Y} = 0, \quad (4)$$

$$\frac{\partial U}{\partial \tau} + U\frac{\partial U}{\partial X} + V\frac{\partial U}{\partial Y} = -\frac{\partial P}{\partial X} + \frac{1}{\mathrm{Re}}\left(\frac{\partial^2 U}{\partial X^2} + \frac{\partial^2 U}{\partial Y^2}\right), \quad (5)$$

$$\frac{\partial V}{\partial \tau} + U\frac{\partial V}{\partial X} + V\frac{\partial V}{\partial Y} = -\frac{\partial P}{\partial Y} + \frac{1}{\mathrm{Re}}\left(\frac{\partial^2 V}{\partial X^2} + \frac{\partial^2 V}{\partial Y^2}\right) + \frac{1}{Fr^2}\left[\phi^2 - 2\phi\right], \quad (6)$$

$$\frac{\partial \phi}{\partial \tau} + U\frac{\partial \phi}{\partial X} + V\frac{\partial \phi}{\partial Y} = \frac{1}{\mathrm{Re}\,\mathrm{Pr}}\left(\frac{\partial^2 V}{\partial X^2} + \frac{\partial^2 V}{\partial Y^2}\right). \quad (7)$$

The domain in this study as shown in Figure 2, consists of a domain width L of total $L = 300$, i.e., $-150 \le X \le +150$, and a domain height $H = 90$ i.e., $0 \le Y \le 90$. The undisturbed, homogeneous medium initial conditions are applied such that

$$U = 0, V = 0, \phi = 0 \text{ for } \tau < 0. \quad (8)$$

For $\tau \ge 0$, the boundary conditions are set such that on the side walls:

$$U = 0, V = 0, \frac{\partial \phi}{\partial X} = 0. \quad (9)$$

At the plume source:

$$Y = H : \begin{cases} U = 0, V = 0, \phi_{in} = 2 \text{ for } X = -150 - 0 \\ \phi_{in} = 0 \text{ for } X = 0 - 150. \end{cases} \quad (10)$$

At the top and base of the domain:

$$U = 0, V = 0, \frac{\partial \phi}{\partial Y} = 0. \quad (11)$$

The simulations are carried out over the ranges of Reynolds number $5 \le \mathrm{Re} \le 2000$, Froude number $0.2 \le Fr \le 1$, and with fixed Prandtl number $\mathrm{Pr} = 7$ throughout this study. The dimensionless temperature $\phi_{in} = 2$ on $L/2$ is equivalent to a discharge at 8°C into an ambient at 0°C. Numerical solution of the above equations is by means of COMSOL Multiphysics Software. This commercial package uses a finite element solver with discretization by the Galerkin method and stabilization to prevent spurious oscillations. We have used the "Extra fine" setting for the mesh. Time stepping is by COMSOL's Backward Differentiation Formulas. Further information about the numerical methods is available from the COMSOL Multiphysics website [29]. Results will be illustrated mainly by surface temperature plots of dimensionless temperature on a colour scale from dark red for the ambient temperature $\phi = 0$, through yellow to white for the source temperature $\phi = 2$. Note that $\phi = 1$ corresponds to the temperature of maximum density, while $\phi = 2$ is the temperature at which warm water has the same density as the ambient cold water.

III. RESULTS

The behaviour of warm discharges through lock-exchange in cold fresh water had been investigated over the ranges of Reynolds number $5 \le \mathrm{Re} \le 2000$, Froude number $0.2 \le Fr \le 1$, and fixed Prandtl number $\mathrm{Pr} = 7$ throughout this study. However, the evolution of temperature field for $\mathrm{Re} = 5 \& 500$ at $Fr = 0.2 \& 1$ is shown in Figure 3 – Figure 6 within different time intervals for effective analysis. The simulation commenced when the two bodies of water were assumed to be homogeneous and quiescent, but almost immediately after the release of these water masses, we observed the commencement of a cabbeling process, that forms a vertical line at the contact point between the two water masses. It is clearly observed that the mixture that have become denser or mixed up to T_m descending to the floor of the container (see Figure 3(a), Figure 4(a), Figure 5(a & b) and Figure 6(a)). As time progresses, we can also observe the development of Rayleigh-Taylor instability on the thermal bar as denser fluid descends to the floor. This makes the entire mixing process more chaotic, though, the instability keeps the vertical orientation of the front separating the masses of water with the temperatures greater and less than 4°C. The rate of mixing at the thermal bar for lower Froude numbers appears intense, and this in turn leads to quick production of denser fluid (see Figure 3 & 4). Whereas, the rate of development or the intensity of this instability reduces as Froude number increases (see Figures 5 & 6), and takes longer time to produce denser fluid that descends as compared to those in Figures 3 & 4. The possible cause of this difference in the mixing is that, the buoyancy term in equation (6) gives the insight that simulations with lower Froude numbers have greater buoyancy and as such could mix faster than those with higher Froude numbers that tend to mix slowly as a result of the reduced buoyancy force. Though, the various contributions that arises as Reynolds number increases (inertial force) cannot also be ignored. Therefore, such flows are always unstable, as it possesses high downward motion as much denser fluid is produced within short period that sinks. This unstable behaviour of the downwelling fluid causes a deviation from the vertical thermal bar, and its intensity in turn perturbs the denser fluid that is already on the floor.

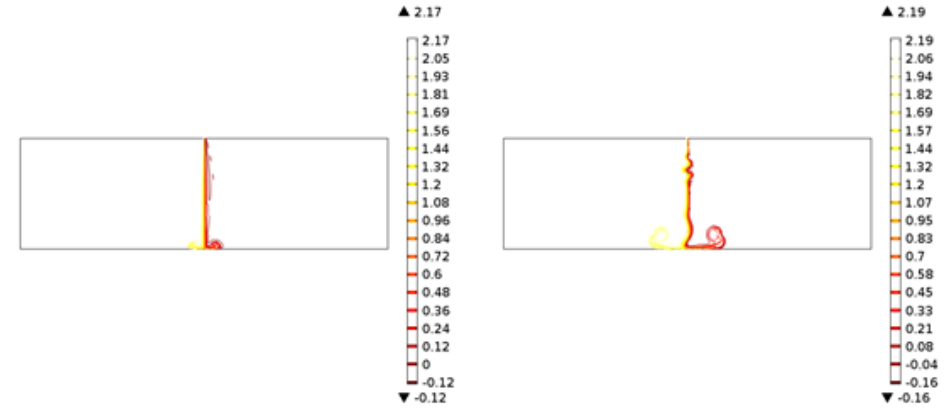

(a) Re = 5 at τ = 2 (b) Re = 5 at τ = 4

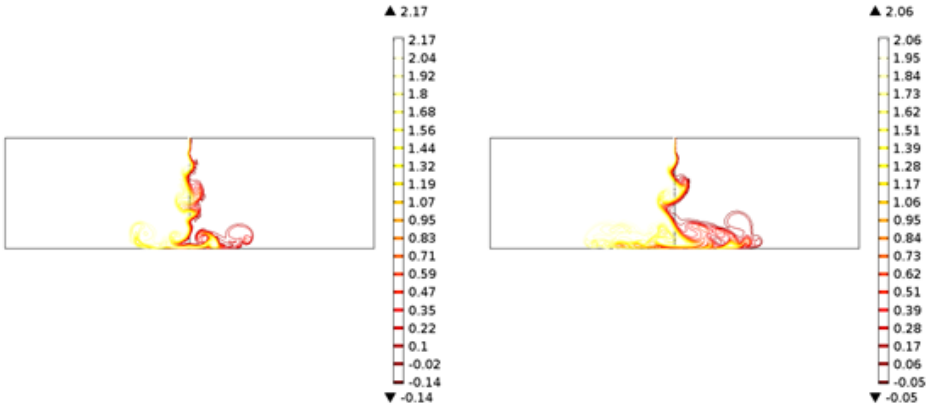

(c) Re = 5 at τ = 6 (d) Re = 5 at τ = 8

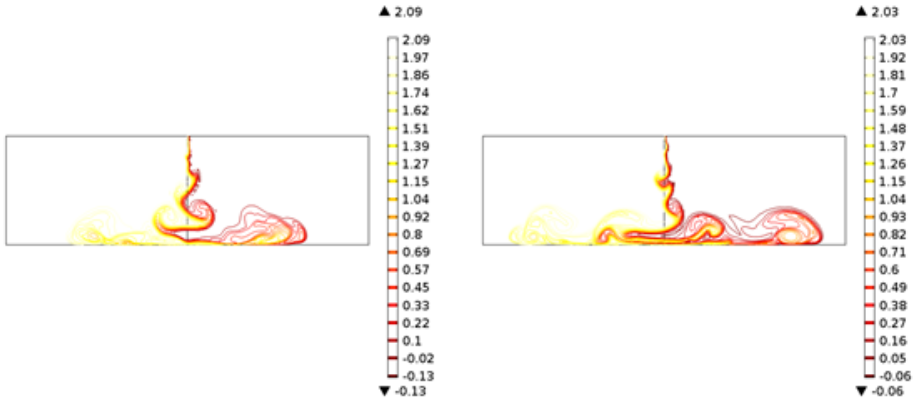

(e) Re = 5 at τ = 10 (f) Re = 5 at τ = 12

Figure 3: Evolution of temperature field in the thermal bar for F r = 0.2 and Reynolds number Re = 5 at time 2 ≤ τ ≤ 12

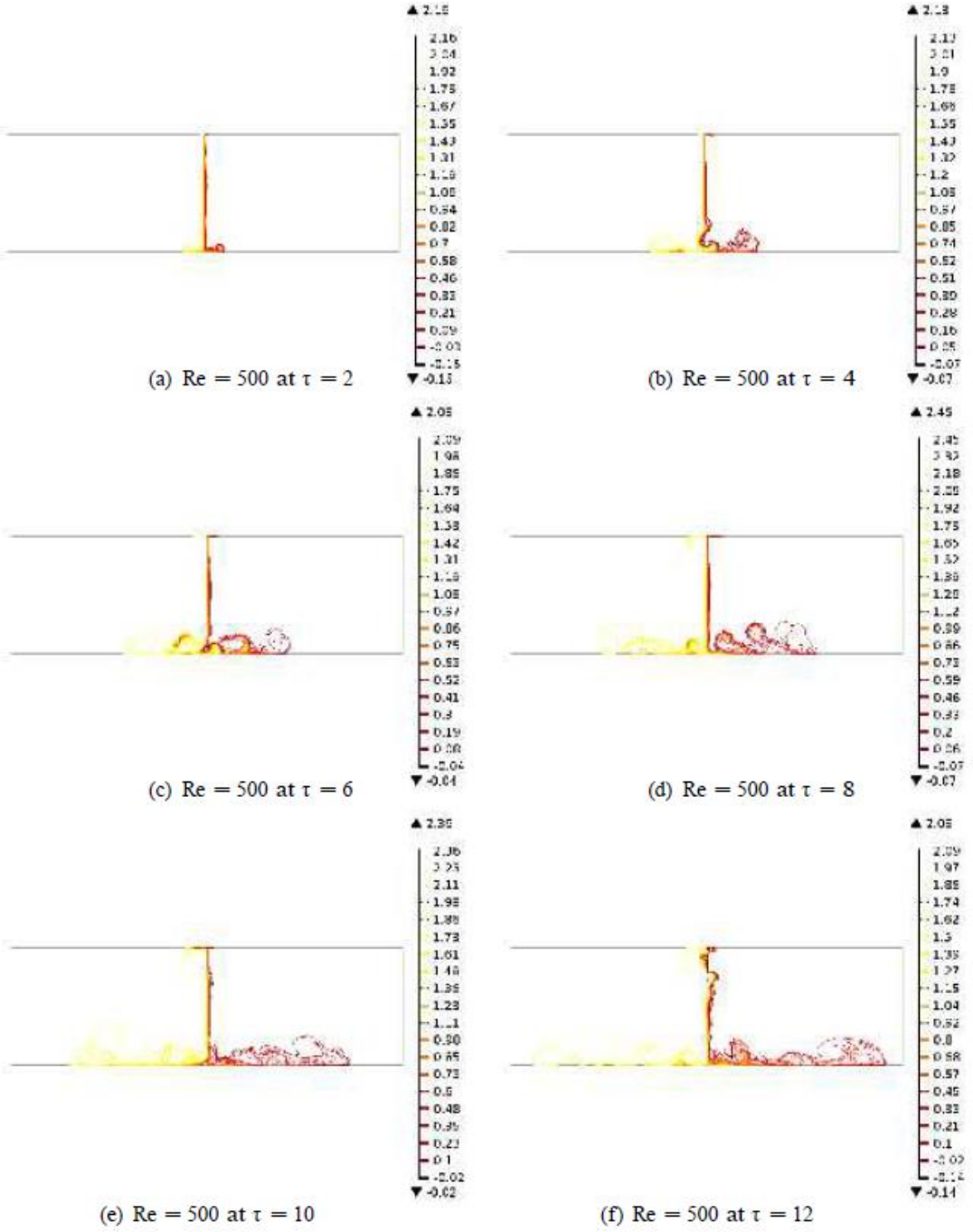

Figure 4: Evolution of temperature field in the thermal bar for $Fr = 0.2$ and Reynolds number $Re = 500$ at time $2 \leq \tau \leq 12$

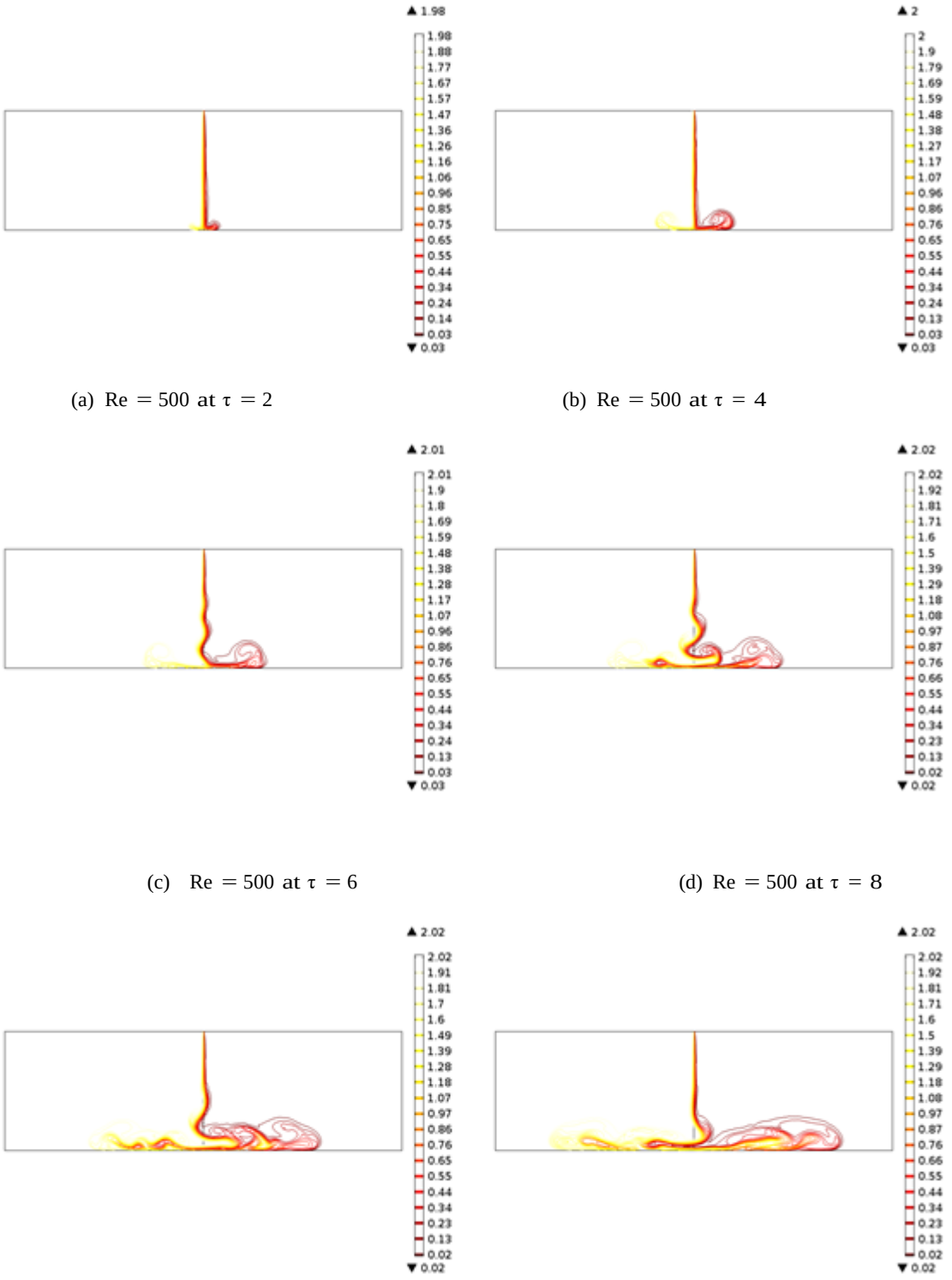

(a) Re = 500 at $\tau = 2$

(b) Re = 500 at $\tau = 4$

(c) Re = 500 at $\tau = 6$

(d) Re = 500 at $\tau = 8$

(e) Re = 500 at $\tau = 10$

(f) Re = 500 at $\tau = 12$

Figure 5: Evolution of temperature field in the thermal bar for F r = 1 and Reynolds number Re = 5 at $10 \leq \tau \leq 60$

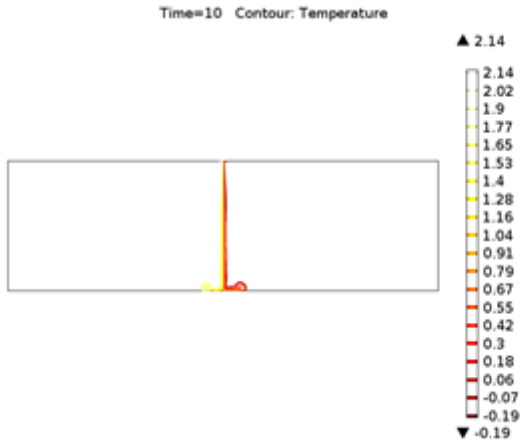

(a) Re = 500 at τ = 10

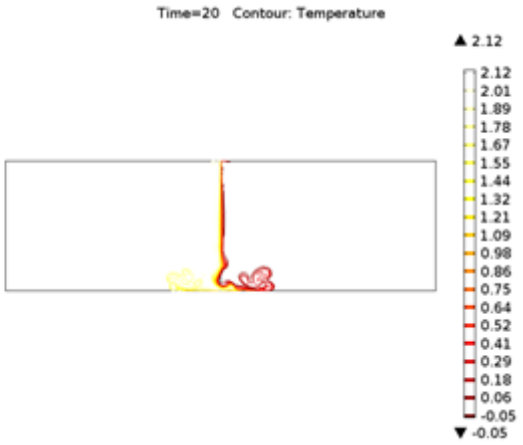

(b) Re = 500 at τ = 20

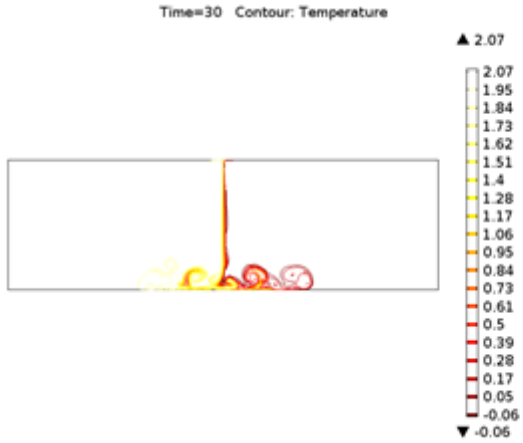

(c) Re = 500 at τ = 30

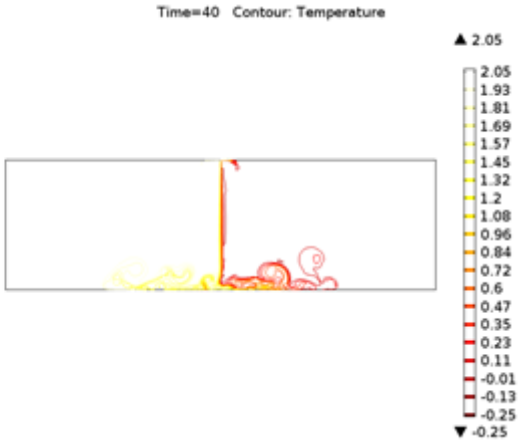

(d) Re = 500 at τ = 40

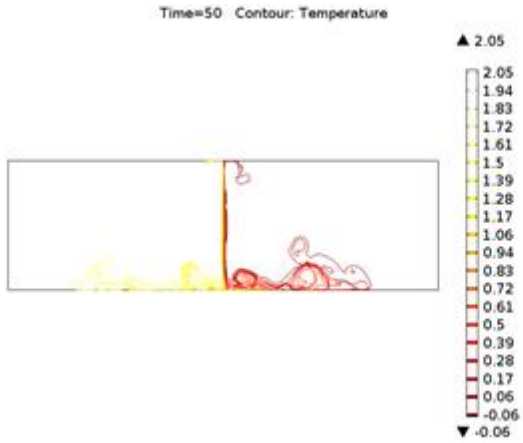

(e) Re = 500 at τ = 50

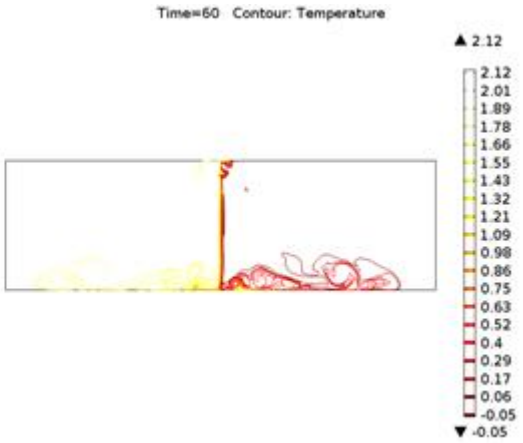

(f) Re = 500 at τ = 60

Figure 6: Evolution of temperature field in the thermal bar for F r = 1 and Reynolds number Re = 500 at 10 ≤ τ ≤ 60

The denser fluid on the floor at the initial time is smooth with a leading head that displaces the ambient fluid as it spreads further (see Figure3(a & b), Figure 4(a), Figure 5(a, b & c) and Figure 6(a)), but later develop large scale instabilities (Kelvin-Helmholtz instabilities in the density current) as it continues to spread. It is also interesting to note here that there is a region very close to the floor where vigorous mixing behaviour is observed (at the base of the container where these two water masses meets (see Figure 3(d) - (f),, Figure 4(b) - (f), Figure 5(d) - (f) and Figure 6(b) - (f))). This is because of the interaction between the Rayleigh-Taylor and Kelvin-Helmholtz instabilities. As the mode of Rayleigh-Taylor instability increases with time while denser fluid descends to the bottom (Figure 3(a) -(d)), so the Kelvin-Helmholtz instability increases with time on the floor, but makes the front of the denser water to be more inclined (see Figure 4(d)). At the point of interaction between the two instabilities, the Rayleigh-Taylor instability frequently move to restore the shape of the thermal bar very close to the floor of the container. This is achieved when the intensity of the motion in Rayleigh-Taylor instability prevails (see Figure 4(d - f) and Figure 6(c - f)). Whereas, if the Kelvin-Helmholtz instability prevails at the point of interaction, then the thermal bar shifts towards the warmer water region on the left, causing constant deformation of the thermal bar and changes in its position at the bottom (see Figure 3(e & f) and Figure 5(d - f)).

Behaviour of the thermal bar is also shown for Reynolds number Re = 5, 50, 500 & 2000 at F r = 0.5 in Figure 7. The results here also show some degree of instabilities in the thermal bar, and this behaviour increases with Reynolds number. This is as a result of the greater inertial force as Reynolds number increases, but comparisons to the results in Figure 3 - Figure 6, indicate that the instability in the thermal bar decreases with increasing Froude number. Development of Kelvin-Helmholtz instability is also apparent, where the prevailing Kelvin-Helmholtz instability had caused a shift of the thermal bar towards the left hand side at some point very close to the base of the container (see Figure 7(a)). Whereas, in Figure 7(b) - (d) the Rayleigh-Taylor instability could restore the thermal bar at this simulation time, but density current spreads out with a leading head that displaces the ambient fluid as it spreads further. The penetration length of the density current for higher Reynolds number shows lengthier as compared to the simulation with the lower Reynolds numbers (see Figure 7). In the same manner, the penetration length of the density current for simulations with lower Froude numbers appears lengthier as compared to those with higher Froude number. As it has been stated earlier, the reason behind this behaviour is that the lower Froude numbers have greater buoyancy and in turn leads to intense mixing, therefore, denser water is produced most rapidly. In the same way, the higher Reynolds number have greater inertial forces that triggers intense mixing.

The behaviour as observed in the results show some similarities with the experimental results obtained by Bukreev [22], where the author also observed Rayleigh-Taylor instability in the thermal bar and Kelvin- Helmholtz instability in density current. The behaviour in the interaction between the two instabilities were also recorded, where the Kelvin-Helmholtz instability makes the initially vertical front of the density current to be more inclined, and the Rayleigh-Taylor instability tends to restore the vertical front of the thermal bar. The author further confirmed that as a result of the interaction between the two instabilities, the thermal bar constantly changes its form and spatial position. Whereas, If the Kelvin-Helmholtz in- stability prevails, the thermal bar shifts towards shallow water, and this is noted as the warm water region.

In order to again more insight into the behaviour of the density current, profiles of temperature and the various velocity components on the density current at the height Y = 3 are also examined, and shown in Figure 8, Figure 9 and Figure 10, for the simulations with Reynolds number Re = 5 & 500 and at Froude number F r = 0.2 as labelled (a) and (b). Based on the vigorous mixing within the thermal bar, significant amount of denser water could be found on the floor even

at the earliest time τ = 2 for both simulations in Figure 8(a) & (b) The profiles of temperature (Figure 8(a) & (b)) also show that the region (Y = 3) as examined contains denser fluid that is of different temperatures depending on the time that is into consideration, but slightly warmer water that is above were observed within the time τ = 4 & 6 at some point closed to the thermal bar (see Figure 8(b)). Similarly, Figure 8(a) also records this warmer water that is above within the time τ = 6 & 10 at some distance away from the thermal bar. Most importantly and irrespective of the time considered, it is clear that all the fluid in this region is denser than both the ambient and the discharge water. Though, reason for the difference in temperatures at the various times is that cabbeling process occurs at all points, where water masses come in contact, and just small degree of mixing is required for denser water to be produced. As such, warm but denser water is likely to descend to the floor most quicker from the region in the thermal bar very close to the floor. Whereas, the cabbeling water that is descending at some point close to the surface may mix up to T_m before reaching the floor. However, the temperature profile here decreases non-monotonically within the current, and the warmest water penetrates farther even as it mixes with the ambient water. Profiles of horizontal velocity components (Figure 9(a) & (b)) for the various Reynolds numbers also gives an explicit description of the density current. The backward flow towards the central part of the thermal bar in the density current because of the Kelvin-Helmholtz instability reaches its greatest speed near X = 255, and an outward flow beyond X =200 for simulations with Re = 5(see Figure 9(a)). Whereas, the backward flow towards the central part is not evident in the simulation with Re =500, because the Rayleigh-Taylor instability always prevails whenever the two instabilities interact, but the outward flow reached its greatest speed within X=175 (see Figure 9(b)). The same is applicable to the profiles of vertical velocity components (Figure 10), though, the downward velocities here are the most densed fluid and are found at the lower part of the density current. This most dense fluid is mainly apparent near the regions of X = 175 & 164 for the simulations with Re = 5 (see Figure 10(a)).

Profiles of vertical velocity component in the thermal bar for the various Reynolds numbers simulation is also shown (see Figure 11(a) & (b)). The downwards motion of the denser water for simulation with Reynolds number Re =500 is higher than that with Re =5, and was recorded within the height Y = 5 − 15 at all times as shown, and beyond this point a decrease in downwards speed was recorded up to the top. Whereas, this downwards motion was not too great for the simulations with Re =5 within the height Y = 5 – 15, but fluctuates upwards as the velocity decreases further. The different behaviour in this Profiles of vertical velocity component in the thermal bar, further confirm the fact that much denser water is produced for the simulation with higher Reynolds number based on the intensity of the mixing process as a result of their greater inertial and buoyancy forces that arises from both the Reynolds number and the lower Froude number. So, the mixture here mixes most rapidly to attain. Unlike the simulations with Re = 5 that have very reduced inertial forces, so the cabbeling process here is bound to occur very slowly, leading to the less production of denser water that descends.

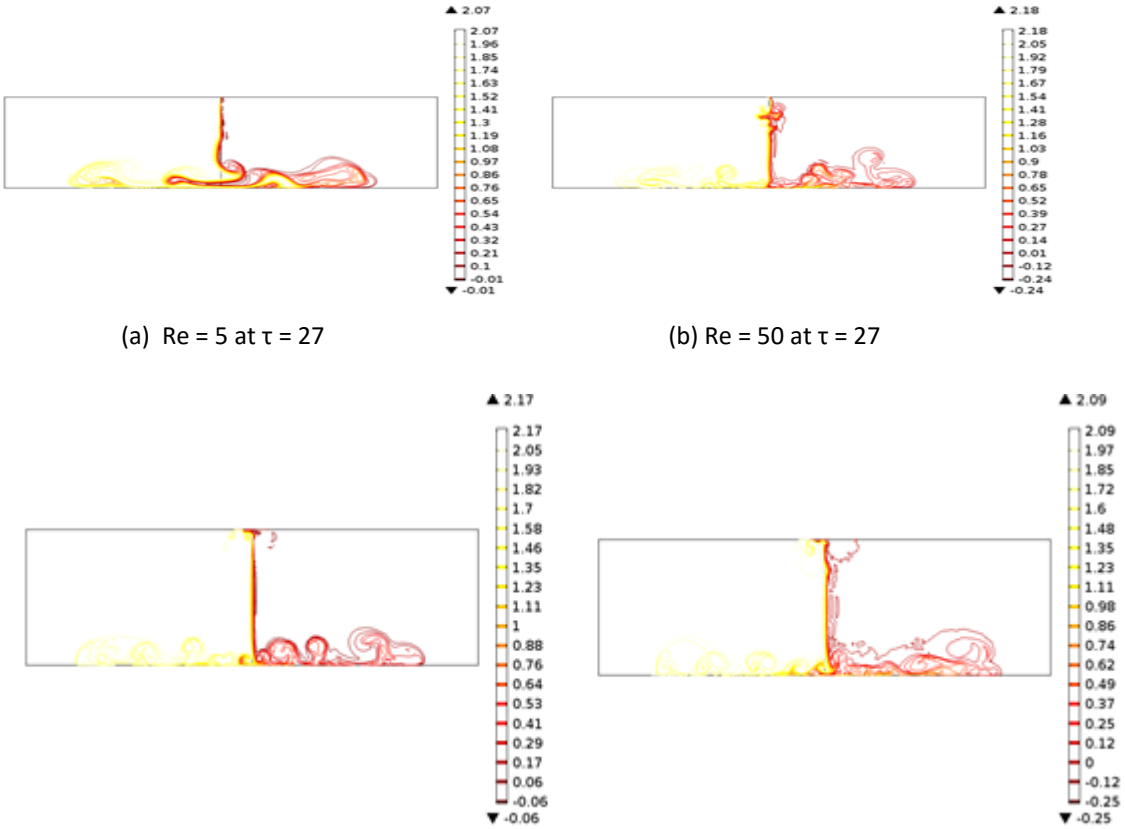

(a) Re = 5 at τ = 27 (b) Re = 50 at τ = 27

(c) Re = 500 at τ = 27 (d) Re = 2000 at τ = 27

Figure 7: Temperature field in the thermal bar for Fr = 0.5 and Reynolds number Re =5, 50, 500 & 2000 at time τ = 60

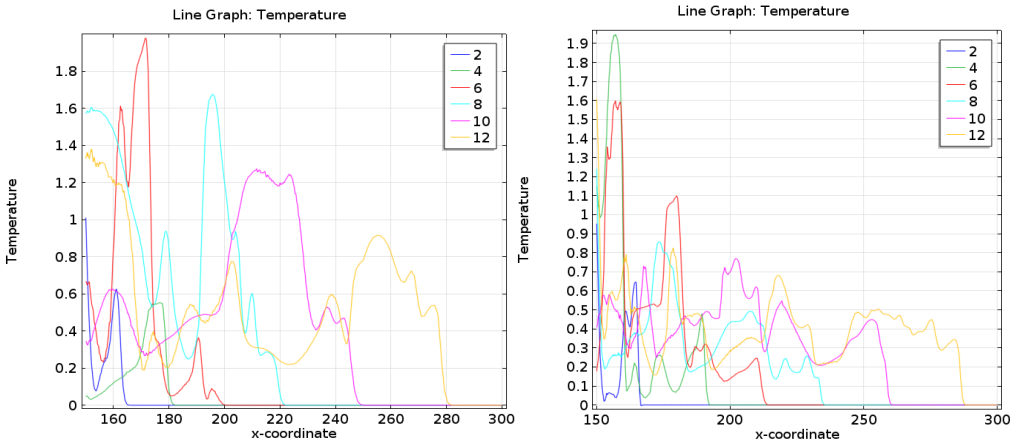

(a) Re = 5 and F r = 0.2 (b) Re = 500 and F r = 0.2

Figure 8: Dimensionless temperature profiles on the floor $\phi(X, 3)$ at time τ = 2, 4, 6, 8, 10, 12 for plumes with Re = 5 &500, P r = 7, $\phi_{in} = 2$ and for F r = 0.2

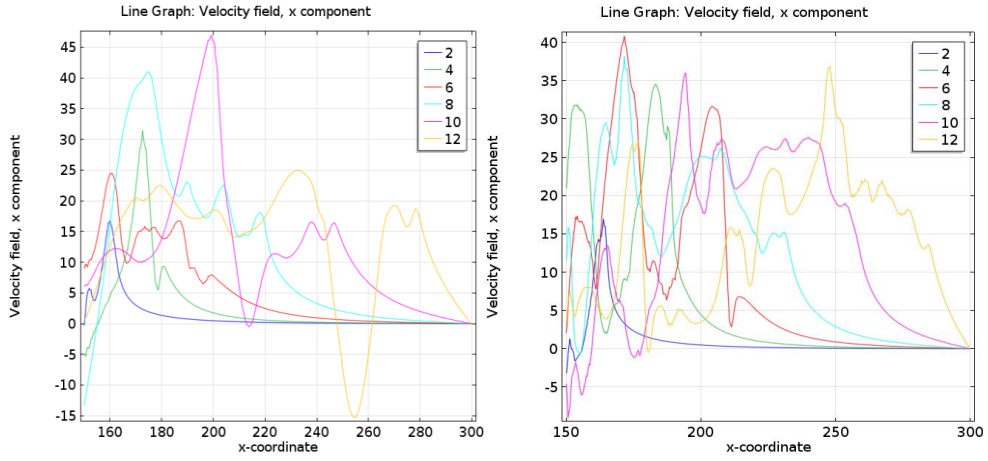

(a) Re = 5 and F r = 0.2 (b) Re = 500 and F r = 0.2

Figure 9: Dimensionless horizontal velocity profiles on the floor $\phi(X,3)$ at time τ=2, 4, 6, 8, 10, 12 for plumes with Re = 5 & 500, P r = 7, $\phi_{in} = 2$ and for F r = 0.2

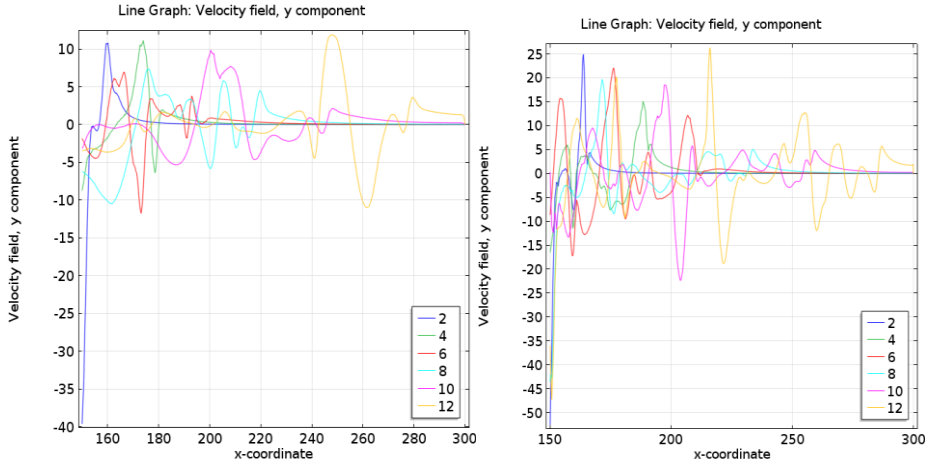

(a) Re = 5 and F r = 0.2 (b) Re = 500 and F r = 0.2

Figure 10: Dimensionless vertical velocity profiles on the floor $\phi(X,3)$ at time τ=2, 4, 6, 8, 10, 12 for plumes with Re = 5 & 500, P r = 7, $\phi_{in} = 2$ and for F r = 0.2

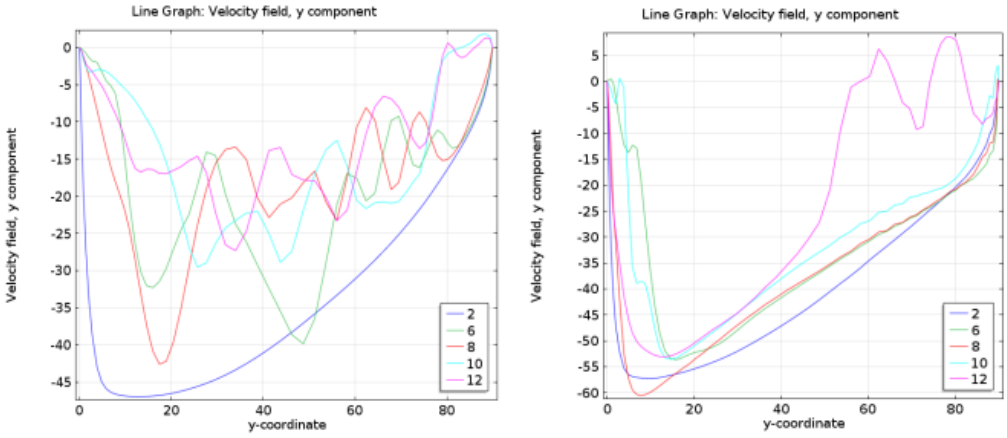

(a) Re = 5 and F r = 0.2 (b) Re = 500 and F r = 0.2

Figure 11: Dimensionless velocity profiles on the centreline at time τ=2, 4, 6, 8, 10, 12 for plumes with Re = 5 & 500, P r = 7, and for F r = 0.2

IV. CONCLUSION

We have investigated the cabbeling behaviour of a thermal bar as denser water descends to the floor using the assumption that the density is a quadratic function of temperature. The results obtained in this paper are very similar to the experimentally studied case by Bukreev [22] and are directly comparable. Rayleigh-Taylor instability in the thermal bar and Kelvin-Helmholtz instability in density current where observed in both cases. The situation where the interaction between the two instabilities causes a deformation in the thermal bar such that the Rayleigh-Taylor instability frequently restores the vertical front of the thermal bar, while the Kelvin-Helmholtz instability destroys the thermal bar whenever it prevails over the Rayleigh-Taylor instability was visibly seen. This process was observed to cause a shift in the thermal bar towards the warm water region. It is pertinent to state here, however, that these behaviours as explained which are all apparent in the results of this paper, were not clearly observed in the experimental study by Bukreev [22]. It must be emphasized further that the behaviours as explained are seen mostly to dependent on the source parameters as they vary and the source temperature at $\phi = 2$. If the temperature $\phi > 2$, the thermal bar would have been formed within the first few time interval, but the lighter water will override the ambient water and form a surface gravity current (see Bukreev [32]). Apart from the general behaviour of both results, the investigations here were able to present profiles of temperature and both velocity components in the density current at some point above the floor, and this gives more insight to the flow behaviour. In a similar manner, profiles of vertical velocity component were also examined in the thermal bar so as to fathom the behaviour in the downward motion. Whereas, Bukreev [22] did not give detailed explanations on both profiles of temperature and the various velocity components in the density current and as well as the thermal bar.

REFERENCES

[1]. Zilitinkevich, S. S., Kreiman, D. K. and Terzhevik, Yu. A. (1992). The Thermal Bar. Journal of Fluid Mechanics, 236 Pp. 27 - 42.

[2]. Marmoush, Y. R., Smith, A. A. and Hamblin, P. F. (1984). Pilot experiments on thermal bar in lock exchange flow. Journal of Energy Engineering, 110 3 Pp. 215 - 227.

[3]. Bukreev, I. V. (2006). Effect of the Nonmonotonic Temperature Dependence of Water Density on the Propagation of a Vertical Plane Jet. Journal of Applied Mechanics and Technical Physics, 47(2)Pp. 169 - 174.

[4]. Turner, J. S. (1966). Jets and Plumes with Negative or Reversing Buoyancy. Journal of Fluid Mechanics, 26 Pp. 779-792.

[5]. George, M. A. and Kay, A. (2016). Warm discharges in cold fresh water: 2. Numerical simulation of laminar line plumes. Journals of Environmental Fluid Mechanics doi:10.1007/s10652-016-9468-x

[6]. Foster, T. D. (1972). An analysis of the Cabbeling instability in Sea water. Journals of Physical Oceanography, 2 (3), Pp. 294-301.

[7]. Bukreev, I. V. and Gusev, A.V. (2011). The effect of densification during mixing on the spreading of a vertical round jet. Doklady Earth Sciences, Pp. 1002 - 1005.

[8]. [8] Bukreev, I. V. (2005). Effect of tan Anomalous Temperature Dependence of the water Density on Circular Jet Propagation. Journals of Fluid Dynamics, 40 (2), Pp. 202 - 208.

[9]. Forel, F. A. (1880). La conge´lation des lacs suisses et savoyards pendant l'hiver 1879-1880. §11. Lac Le´man. L'E´ cho des Alpes, 3 Pp. 149 - 161

[10]. Holland,R. P. and Kay, A. (2003). A review of the physics and ecological implications of the thermal bar circulation. Limnologica, 33 Pp. 153 - 162.

[11]. Holland, R. P., Kay, A. and Botte, V. (2003). Numerical modelling of the thermal bar and its ecological consequences in a river-dominated lake. Journal of Marine Systems, 43 Pp. 61 - 81.

[12]. Rao, R. Y., Skafel, G. M. and Charlton, N. M. (2004). Circulation and Turbulent Exchange Characteristics during the Thermal bar in Lake Ontario. Limnology and Oceanography, 49 (6), Pp. 2190 -2200.

[13]. Arifin, R. R., James, C. S., de Alwis Pitts, A. D., Hamlet, F. A., Sharma, A. and Fernando, S. J. H. (2016). Simulating the thermal behavior in Lake Ontario using EFDC. Journal of Great Lakes Research, 42, Pp. 511 - 523.

[14]. Gbah, B. M., Jacobs, J. S., Meadows, A. G. and Bratkovich, A. (1998). A Model of the Thermal bar circulation in a long Basin. Journals of Geophysical Research, 103 (C6), Pp. 12807 - 12821.

[15]. Farrow, E. D. (1995). A Numerical Model of the Hydrodynamics of the Thermal bar. Journal of Fluid Mechanics, 303, Pp. 279 - 295.

[16]. Holland, R. P., Kay, A. and Botte, V. (2001). A Numerical Study of the Dynamics of the Riverine Thermal Bar in a Deep Lake. Environmental Fluid Mechanics, 1 Pp. 311 - 332.

[17]. Fossati, M., Santoro, P., Urrestarazu, S. and Piedra-Cueva, I. (2011). Numerical Study of the Effect of a Power Plant Cooling Water Discharge in the Montevideo Bay. Journal of Applied Mathematics, Pp. 1-23

[18]. Agarwal, K. R. and Sangal, K. V. (2008). Krishna's Environment and Ecology. First edition India, Krishna Prakashan Media (P) Ltd.

[19]. Macqueen, J. F. (1979). Turbulence and cooling water Discharges from Power Stations. In Mathematical Modelling of Turbulent Diffusion in the Environment. (ed. C. J. Harris,) Pp. 379-437

[20]. Sharma, K. B. and Kaur, H. (1993). Thermal and Radio Active Pollution. First edition India, Krishna Prakashan Mandir.

[21]. Bukreev, I. V. (2004). Hydrodynamic Instability Caused by the Anomalous Temperature Dependence of the Water Density. Doklady Physics, 49(6) Pp. 393 - 395.

[22]. Bukreev, I. V. and Gavrilov, V. N. (2010). Instability of the Thermal Bar Formed in a Gravity Current. Doklady Earth Sciences, 430 Part 1, Pp. 151 - 154

[23]. Bukreev, I. V. (2011). Plunging Current Caused by Nonmonotonous Water Density Dependence on Temperature. Oceanology, 51(4) Pp. 612 - 620.

[24]. Bukreev, I. V. and Gusev, V. A. (2012). Effect of the Nonmonotonic Temperature Dependence of Water Density on Convection Under Uniform Heating. Journal of Applied Mechanics and Technical Physics, 53(5) Pp. 664 - 671.

[25]. Bukreev, I. V. and Gusev, V. A. (2012). Influence of Anomalous Temperature Dependence of Water Density on Convection at Lateral Heating. Thermophysics and Aeromechanics, 19(4) Pp. 579 - 588.

[26]. Bukreev, I. V. (2005). Effect of the Anomalous Temperature Dependence of Water Density on Surface Gravity Current. Journal of Applied Mechanics and Technical Physics, 46(1) Pp. 49 - 54.

[27]. Bukreev, I. V. (2006). Effect of the Nonmonotonic Temperature Dependence of Water Density on the Decay of an initial Discontinuity. Journal of Applied Mechanics and Technical Physics, 47(1) Pp.54 - 60.

[28]. Hoglund, B. and Spigarelli, S. A. (1972). Studies of the Sinking Plume Phenomenon. In Proc. 15th Conf. Great Lakes Res, Pp. 614-624. International Association of Great Lakes Research.

[29]. COMSOL Multiphysics Cyclopedia. The Finite Element Method (FEM). [ONLINE] Available at: https://www.comsol.com/multiphysics/finite-element-method [Accessed 28 April 2016].

[30]. Moore, D. R. and Weiss, N. O. (1973). Nonlinear penetrative convection. Journal of Fluid Mechanics, 61 Pp. 553 - 581.

[31]. Oosthuizen, P. H. and Paul, J. T. (1996). A Numerical study of the Steady State Freezing of Water in an open Rectangular Cavity. International Journal of Numerical Methods for Heat and Fluid Flow, 6 (5), Pp. 3-16

[32]. Bukreev, I. V. (2006). Effect of the Nonmonotonic Temperature Dependence of Water Density on the Propagation of a Vertical Plane Jet. Journal of Applied Mechanics and Technical Physics, 47 (2) Pp.169 - 174.